Research Article

Arshad H. Khan, Lydia K. Lee, and Desmond J. Smith*

Single-cell analysis of gene expression in the substantia nigra pars compacta of a pesticide-induced mouse model of Parkinson's disease

https://doi.org/10.1515/tnsci-2022-0237
received May 26, 2022; accepted July 25, 2022

Abstract: Exposure to pesticides in humans increases the risk of Parkinson's disease (PD), but the mechanisms remain poorly understood. To elucidate these pathways, we dosed C57BL/6J mice with a combination of the pesticides maneb and paraquat. Behavioral analysis revealed motor deficits consistent with PD. Single-cell RNA sequencing of substantia nigra pars compacta revealed both cell-type-specific genes and genes expressed differentially between pesticide and control, including *Fam241b*, *Emx2os*, *Bivm*, *Gm1439*, *Prdm15*, and *Rai2*. Neurons had the largest number of significant differentially expressed genes, but comparable numbers were found in astrocytes and less so in oligodendrocytes. In addition, network analysis revealed enrichment in functions related to the extracellular matrix. These findings emphasize the importance of support cells in pesticide-induced PD and refocus our attention away from neurons as the sole agent of this disorder.

Keywords: basal ganglia, maneb, paraquat, neurodegeneration, scRNA-seq

1 Introduction

Parkinson's disease (PD) ranks as the second most common neurodegenerative disorder [1]. The disease affects approximately 2–3% of the world population over 65 years of age and the risk of PD increases with age. In the US alone, more than one million people have PD and about 50,000 new cases are diagnosed yearly. The cardinal signs of the disease are tremor, rigidity, bradykinesia, and postural instability. There are, in addition, a wide variety of other features including cognitive dysfunction, dementia, mood disorders, autonomic dysfunction, and olfactory disturbances. Pathologically, PD is characterized by the loss of dopaminergic neurons in the substantia nigra pars compacta (SNpc) that project to medium spiny neurons in the dorsal striatum [2,3]. Surviving neurons in the SNpc exhibit characteristic inclusions called Lewy bodies, which are comprised principally of α-synuclein protein [4].

Genetics makes a substantial contribution to PD. The heritability of PD due to common variants is ~22%, and 90 such variants have been identified [5]. In addition, more than 20 monogenic loci have been uncovered [6]. However, environment clearly also makes an important contribution to PD. Epidemiological studies have shown that exposure to pesticides increases the risk of PD [4,7,8]. In particular, both the fungicide maneb (MN, manganese ethylene-bis-dithiocarbamate) and the herbicide paraquat (PQ) have been associated with PD [9,10].

In mice, either MN or PQ results in the neurodegeneration of dopaminergic neurons by inhibiting mitochondrial function and elevating oxidative stress, a common pathway for PD [10–13]. A well-established mouse model of pesticide-induced PD employs combined dosing of both agents [maneb and paraqua (MNPQ)]. The result is loss of tyrosine hydroxylase neurons in the SNpc, increased α-synuclein aggregates, and abnormalities in motor behavior reminiscent of PD in humans [4,10,14,15].

Transcript profiling of human PD brain samples and animal models has revealed molecular pathways underpinning the disorder. As well as disruption of mitochondrial function and oxidative stress, these pathways include dopamine metabolism, protein degradation, inflammation, vesicular transport, and synaptic transmission [11,16–18].

* **Corresponding author: Desmond J. Smith,** Department of Molecular and Medical Pharmacology, David Geffen School of Medicine, UCLA, Box 951735, 23-151 A CHS, Los Angeles, CA 90095-1735, United States of America, e-mail: DSmith@mednet.ucla.edu
Arshad H. Khan: Department of Molecular and Medical Pharmacology, David Geffen School of Medicine, UCLA, Box 951735, 23-151 A CHS, Los Angeles, CA 90095-1735, United States of America
Lydia K. Lee: Department of Obstetrics and Gynecology, David Geffen School of Medicine, UCLA, Los Angeles, CA 90095-6928, United States of America

More recently, massively parallel single-cell RNA sequencing (scRNA-seq) has deciphered pathways of PD at finer cellular resolution [19]. For example, studies using mouse and human samples have identified specific gene expression changes not only in dopaminergic neurons but also in oligodendrocytes, though not microglia [20–23]. One investigation found early downregulation of HDAC4-controlled genes in an induced pluripotent stem cell model of PD [24].

Despite the increasing use of scRNA-seq to understand PD, this technology has been little employed to decipher the cellular heterogeneity of pesticide-induced PD. In this report, we evaluate the cellular and gene expression changes occurring in the SNpc in a mouse model of PD induced using MNPQ. We obtained a low yield of viable single cells from the SNpc and the data were of marginal quality, despite stringent filtering. Nevertheless, initial insights could be gleaned from the dataset, suggesting potential cellular mechanisms for pesticide-induced PD.

2 Materials and methods

2.1 Animals

A total of 36 C57BL/6J mouse (8 weeks old) were obtained from Jackson Laboratory, Bar Harbor, Maine. Each mouse was housed for 2 weeks (3 per each cage) to allow acclimatization to the new environment.

Ethical approval: The research related to animals' use has been complied with all the relevant national regulations and institutional policies for the care and use of animals. Experiments were ratified by the UCLA Chancellor's Animal Research Committee (ARC-2002-175) and performed following the Guide for the Care and Use of Laboratory Animals published by the United States National Institutes of Health (NIH Publication No. 85-23, revised 1996) and with UCLA Policy 990 on the Use of Laboratory Animal Subjects in Research (revised 2019).

2.2 Pesticide treatment

After acclimatization, mice were treated either with saline (vehicle) or MNPQ (9 males, 9 females in each group). Animals were weighed at 10 weeks of age and intraperitoneal (i.p.) injections of 10 mg kg^{-1} PQ and 30 mg kg^{-1} MN given twice per week (Monday and Friday) for 3 weeks. PQ was administered first, followed an hour later by MN. Control mice received saline under the same regimen. Two females in the MNPQ group died before data could be collected.

2.3 Pole and adhesive (dot) removal test

One week after the administration of MNPQ or saline, motor effects were evaluated in treated and control mice using the pole test and the adhesive (dot) removal test [4,25]. Both tests are established assays of motor deficits in mouse models of PD [15,26,27].

For the pole test, each mouse was placed head-up on top of a vertical wooden pole with a rough surface, 50 cm in height and 1 cm in diameter. The animals were allowed to orient themselves downward and to descend along the pole back into their home cage. Each mouse was exposed to three trials, and the time spent to orient downward (t-turn) and the time to descend (t-descend) were recorded. If the mouse was unable to turn downward, the default value of 120 s was recorded as the maximal severity of impairment. For the adhesive (dot) removal test, each mouse was removed from their home cage and placed them in a testing cage for 60 s. After acclimatization, a 1.3 cm diameter adhesive paper was placed on top of their forehead. Each mouse was given three trials, and the times to touch the dot and to remove the dot were recorded.

Linear mixed models using the `lme4` package in `R` were employed to analyze the pole and adhesive (dot) removal test, with fixed effects of treatment and sex, and a random intercept of individual mouse [28,29]. Significance testing of the fixed effects employed the `emmeans` package in `R` and used a t-statistic with Kenward–Roger degrees of freedom [30]. The alpha significance threshold (P value) was two-sided and set at 0.05. Measurements are quoted as mean ± standard error of the mean.

2.4 Single cell isolation from SNpc

One week after the completion of behavioral testing, the last cohort of mice consisting of three males from the control (vehicle) and three males from the treated (MNPQ) animals were used for single-cell isolation from SNpc. This design was employed to minimize batch effects. Animals were euthanized using isoflurane followed by cervical dislocation. Immediately after euthanasia, the brains were

removed and placed on an ice cold mouse brain matrix (1 mm slices) and the region of 1.28 mm bregma to 2.28 mm bregma containing the SNpc sliced out. Punch dissection was used to dissect out SNpc and single cells dissociated by digestion using 2 mg mL^{-1} papain for 30 min at 34°C followed by trituration for 35 min. Debris was removed by filtration using a 40 mm filter. Cells were pelleted and the supernatant was removed. Cells were resuspended in 1× phosphate-buffered saline with 0.04% fetal bovine serum and quantified and quality checked using a Countess II Automated Cell Counter (Thermo Fisher). A total of 1 mL of cells at ~1,200 cells μL^{-1} were submitted for sequencing.

2.5 scRNA-seq

Sequencing libraries were constructed from isolated single cells of vehicle and MNPQ samples using 10× Genomics Chromium technology with 3′-end gene expression library preparation. An Illumina NextSeq 500 SBS sequencing machine was used with 1 × 75 cycles and paired-end sequences of 26 and 57 bp. Sequence data were demultiplexed and mapped against the indexed mouse reference genome (refdata-cellranger-mm10-3.0.0.tar.gz; GRCm38/mm10) using the Cell Ranger count pipeline software package (10× Genomics). Data from each sample were initially filtered to exclude genes expressed in fewer than five cells and to exclude cells that contained fewer than 100 expressed genes.

To improve quality, strict filtering was further done on the raw data using the Seurat R package with the number of unique molecular identifiers (nUMI) >500, nGene >500, $\log_{10}$GenesPerUMI >0.80 and mitoRatio <0.20 criteria [31]. Normalization and variance stabilization of the scRNA-seq data were done using the SC transform method in Seurat, which corrects for technical factors such as differences in cell numbers and sequencing depth.

2.6 Cell clustering and identification of marker genes

Cell types in each sample were clustered using dimensionality reduction procedures, such as principal component analysis and uniform manifold approximation and projection (uMAP). Graph-based clustering was performed using the Seurat function FindNeighbors and FindClusters. Each cluster was separated using the Leuvain algorithm with a resolution parameter of 0.5. To visualize the clusters, non-linear dimensional reduction was performed using uMAP with the same principal components (PC) employed for the graph-based clustering. The Seurat function FindAllMarkers was used to identify marker genes for the clusters.

2.7 Average expression and differential expression of each marker

The average expression of cell-type-specific markers was calculated using the Seurat package. Markers for each cell types were subset and natural logarithms were taken of average expression of RNA counts plus one. Differential expression of genes and corresponding significance values between control and experimental samples were calculated separately for each cluster using the FindMarkers functions of Seurat package. Adjusted *P* values employed Bonferroni corrections for multiple hypothesis testing.

3 Results

3.1 Pole and adhesive removal test

On the pole test, the MNPQ-treated mice showed significantly greater time to turn around (control mice = 5.0 ± 0.37 s, MNPQ mice = 6.5 ± 0.40 s, $t[1,31] = 2.7$, $P = 0.012$) and also to climb down the pole (control mice = 11.4 ± 0.58 s, MNPQ mice = 13.7 ± 0.62 s, $t[1,31] = 2.8$, $P = 9.5 \times 10^{-3}$) (Figure 1a and b). There was no significant effect of sex for either the turn-around or climb down time.

For the adhesive removal test, there was no significant difference between vehicle and MNPQ-treated mice for time to either touch the dot (control mice = 11.7 ± 1.91 s, MNPQ mice = 15.9 ± 2.03 s, $t[1,31] = 1.52$, $P = 0.14$) or for time to remove the dot (control mice = 13.3 ± 1.99 s, MNPQ mice = 17.9 ± 2.11 s, $t[1,31] = 1.58$, $P = 0.12$). There was no significant effect of sex for either the time to touch or remove the adhesive dot. Nevertheless, the pole test was consistent with the notion that pesticide exposure in mice results in motor deficits reminiscent of PD.

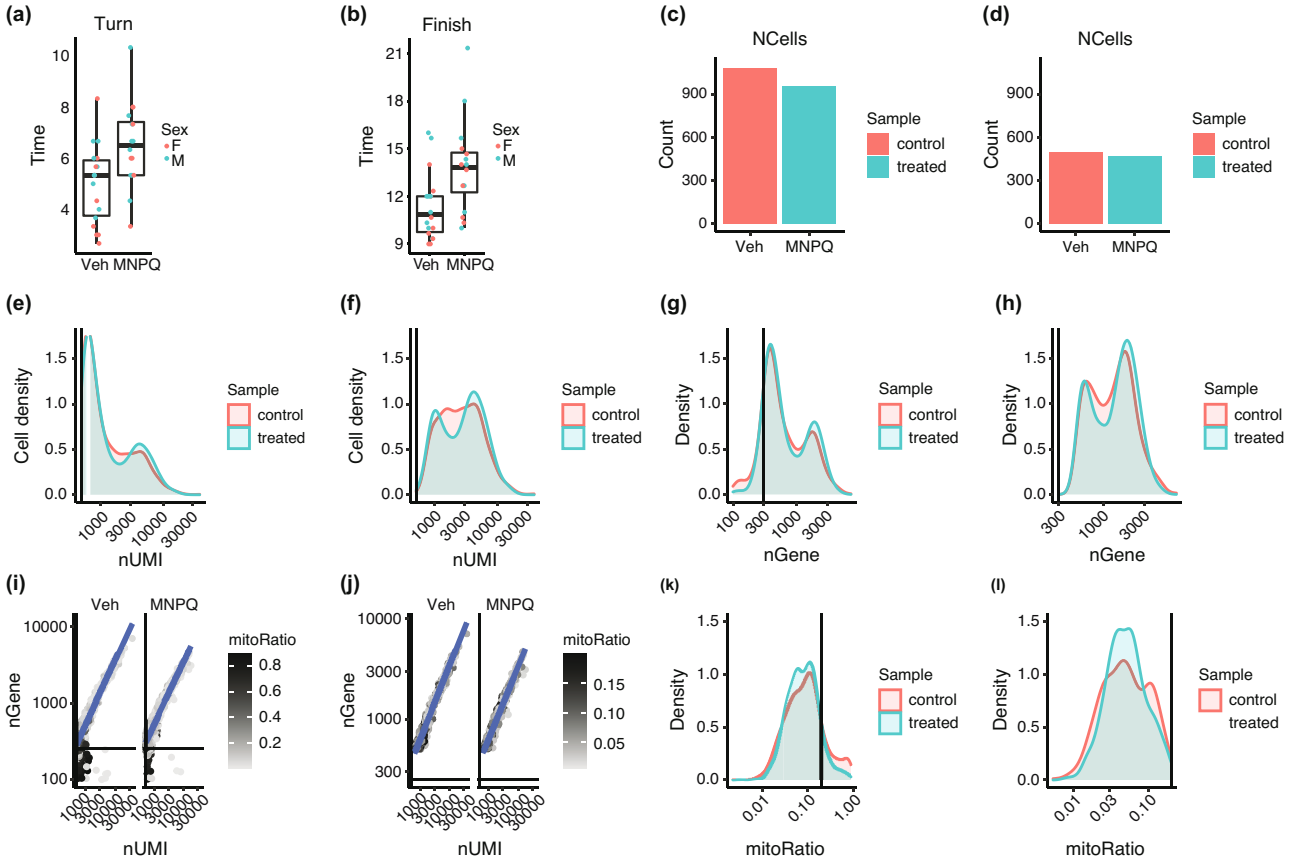

Figure 1: Behavioral testing and data filtering methods. (a) Pole test, time to turn. (b) Pole test, time to finish climbing down pole. Veh, vehicle. Differences between groups for both endpoints, $P < 0.05$. (c) Cell counts using Cell Ranger pipeline. (d) Cell counts using strict filtering removing unwanted cells that are either dead or tagged with ambient RNA. (e) Number of transcripts from Cell Ranger. (f) Number of transcripts from strict filtering. (g) Number of genes per cell obtained by Cell Ranger. (h) Number of genes per cell obtained by strict filtering criteria. (i) High mitochondrial read fractions (dark color) indicate damaged/dead cells due to leaked cytoplasmic mRNA. (j) Mostly live cells after filtering out dead cells. (k) Appreciable numbers of dead cells before strict filtering using mitochondrial read fractions. (l) Dead cells removed after strict filtering.

3.2 scRNA-seq and mapping

Sequencing results are summarized in Table S1. More than 180 and 175 million sequence reads, 1,105 and 965 cells, and 17,480 and 16,908 transcripts were obtained from SNpc of control and MNPQ animals, respectively. The sequencing data showed acceptable quality based on the percentage of bases with Q30 or better in the RNA reads, with scores 64.5 and 63.8% in control and MNPQ samples (ideal threshold is >65%). However, the fraction of reads in cells (the fraction of confidently mapped reads with cell-associated barcodes) was 24.7 and 23.9% for the control and experimental samples (ideal score of >70%).

The poor-quality score for the fraction of reads in cells suggested that many of the reads were not assigned to cell-associated barcodes. Possible causes are high levels of ambient RNA or increased number of cells with low RNA content, preventing the algorithm from calling cells. Ambient RNAs are usually pooled mRNA molecules that have been released in the cell suspension from stressed cells or cells that have undergone apoptosis. Isolation of single cells from mouse SNpc is a tedious process, resulting in many dead cells. Despite the marginal quality of the data, we decided to pursue further analysis in the spirit of an exploratory study.

3.3 Data filtering

We initially filtered the sequence data from each sample using the Cell Ranger pipeline to exclude genes expressed in fewer than five cells and cells containing fewer than 100 expressed genes. However, because of the poor quality of

the scRNA-seq data, we decided to use the Seurat pipeline to impose a stricter threshold than standard. The mitochondrial transcript ratio of each cell was incorporated into the metadata, thus avoiding over representation of mitochondrial genes that possibly represent dead cells [32,33]. We used the following criteria: number of nUMI >500, nGene >500, log10GenesPerUMI >0.80, and mitoRatio <0.20.

We compared the cell counts per sample, UMI counts (transcripts) per cell and genes detected per sample after filtering from the Cell Ranger pipeline or using the strict filtering of the raw data from Seurat (Figure 1c–h). We lost more than half of the cell number as a result of the strict filtering. Using the Cell Ranger filtering criteria, many cells had a UMI count of <500, while the strict filtering criteria selected cells with a UMI count of >500 (Figure 1e and f). A similar pattern was obtained from the number of genes detected per cell (Figure 1g and h). The distributions of UMI and genes per cell were bimodal, whereas a single peak is expected (Figure 1e–h). The bimodal distributions may indicate the presence of biologically different cell types in the data (simpler vs more complex expression profiles) or cells that are larger in size [34,35].

To determine whether the strong presence of cells with low numbers of genes/UMIs were due to mitochondria, we plotted the number of UMIs and the number of genes detected per cell using the Cell Ranger pipeline (Figure 1i–k). The bottom left quadrants of the plots in Figure 1i represent poor-quality cells with a low number of genes and UMIs. High mitochondrial read fractions (dark color) were found in these cells and are probably indicative of damaged/dying cells, which only retain mitochondria mRNA and have leaked cytoplasmic mRNA. The strict filtering (<0.2 mitochondrial ratio) permitted selection of data with very low numbers of dying cells (Figure 1j–l).

The stringent filtering allowed us to remove most of the noise from the data, although almost half of the filtered data (specifically cell numbers) generated by Cell Ranger were lost. The total number of cells dropped to 494 and 468 for control and experimental samples, respectively, and the number of genes dropped to 13,038. However, the strict quality control provided us with more confidence in the downstream analysis.

3.4 Cell clustering

Initial clustering of data from control and treated samples resulted in 13 distinct cell clusters (Figure S1). To identify cell types in each cluster, the top 25 marker genes in each cluster were assessed for cell specificity using a database of cell markers in human and mouse [36]. If 50% or more of the top 25 marker genes belonged to a specific cell type, then the cluster was assigned that cell type. This process reduced the number of clusters to seven (astrocytes, endothelial cells, neuron, microglia, oligodendrocytes, mural cells, and ependymal cells) (Figure 2).

Significant genes in each cell cluster based on expression differences with all other clusters are shown in Table S2. Most of the marker genes were specific for their own cluster except for a few that overlapped. Examples of marker genes for each cell type in the combined samples and the separate MNPQ and control samples are shown using dot plots in Figure 3a and b. Heatmaps of mean expression for all markers in control and treated samples also showed cell-type-specific gene expression (Figure 3c and d).

3.5 Gene markers in clusters

The top three most significant neuronal markers were *Syt1* ($P = 1.91 \times 10^{-56}$, 4.86×10^{-58}), *Snap25* ($P = 1.50 \times 10^{-49}$, 2.72×10^{-47}), and *Rtn1* ($P = 2.90 \times 10^{-47}$ and 9.13×10^{-42}) (adjusted *P* values in MNPQ and control samples, respectively). The *Syt1* protein is thought to interact with α-synuclein and the *Snap25* protein forms part of the SNARE complex [37]. Changes in the abundance and distribution of the SNARE complex impair dopamine-mediated modulation of synaptic function and are involved in PD initiation. *Rtn1* plays a role in neuronal injury in an *in vitro* model of PD using the neurotoxin MPP^+ (1-methyl-4-phenylpyridinium) [38]. Synaptophysin (*Syp*) was another strongly expressed neuronal gene in our study (adjusted $P = 2.19 \times 10^{-46}$ and 1.32×10^{-30} in MNPQ and control samples, respectively) and is a marker of synaptic terminals that shows loss in neurodegenerative disorders such as PD [39].

Astrocyte specific genes included *Gpr37L1* ($P = 1.68 \times 10^{-70}$ and 1.35×10^{-59}), *Pla2g7* ($P = 8.94 \times 10^{-63}$ and 2.63×10^{-52}), and *Prdx6* ($P = 1.01 \times 10^{-48}$ and 4.01×10^{-32}) (adjusted *P* values in MNPQ and control samples, respectively). The protein encoded by *Gpr37L1*, the top astrocyte specific marker, is a G-protein-coupled receptor. Both the *Gpr37L1* protein and its homolog, the PD-associated orphan receptor *Gpr37*, physically interact with the dopamine 2 receptor (*Drd2*), which is expressed in astrocytes as well as neurons [40–42]. The *Gpr37* protein is also a key substrate for *Parkin*, mutations of which cause autosomal recessive juvenile PD [43].

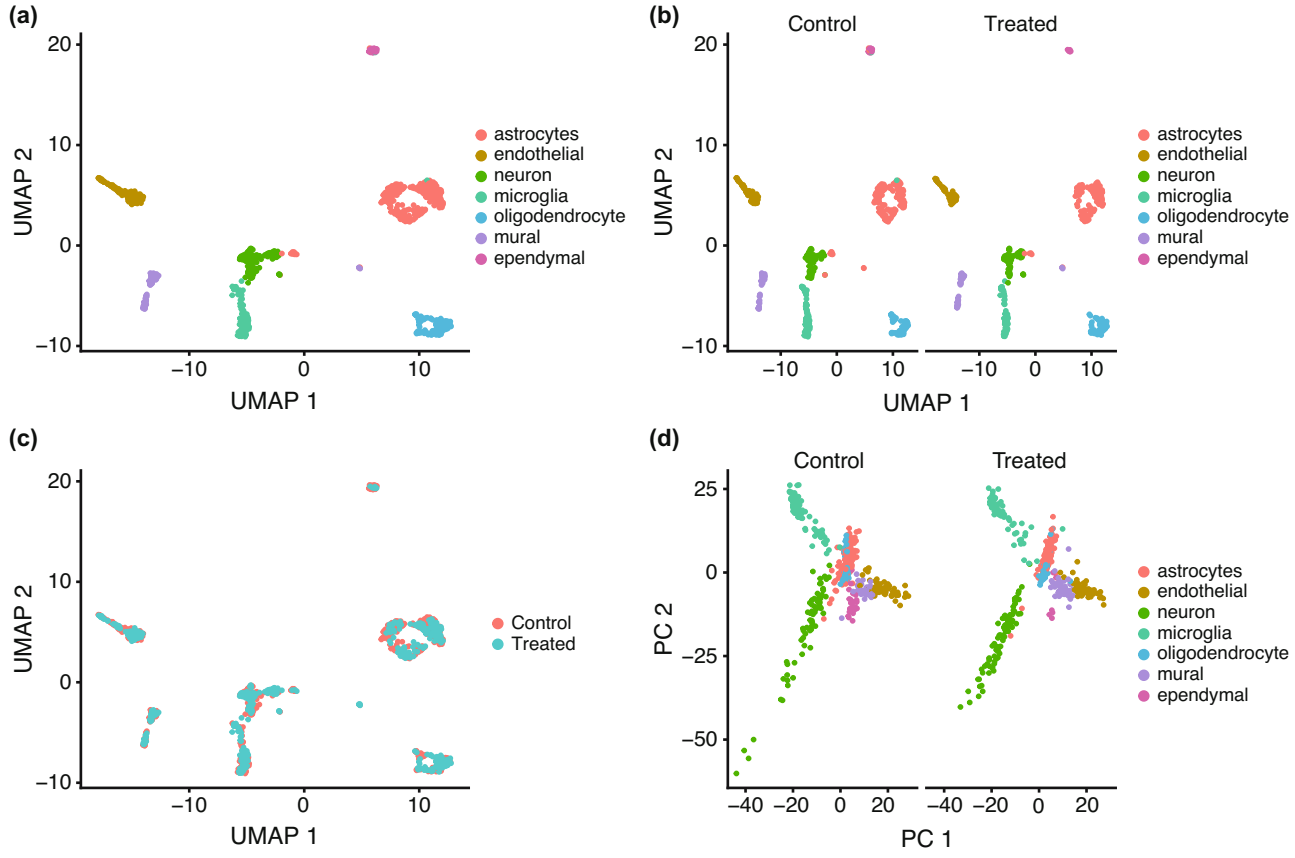

Figure 2: Cell clusters in SNpc from control and MNPQ mice. (a) Seven clusters classified by cell type using UMAP. (b) Clusters separated by sample condition. (c) Overlap of cell clusters between samples. (d) Clusters separated by sample condition using PC.

Mutations in the astrocyte specific gene, *Pla2g7*, cause early-onset PD [44]. In addition, transgenic mice expressing the astrocyte-specific gene, *Prdx6*, show increased loss of dopaminergic neurons and more severe behavioral deficits in the MPTP (1-methyl-4-phenyl-1,2,3,6-tetrahydropyridine) mouse model of PD compared to non-transgenic controls [45].

The top oligodendrocyte-specific markers were *Ermn* ($P = 1.25 \times 10^{-88}$ and 8.87×10^{-87}), *Cldn11* ($P = 4.70 \times 10^{-86}$ and 3.50×10^{-88}), and *Ugt8a* ($P = 1.08 \times 10^{-73}$ and 4.33×10^{-88}) (adjusted P values in MNPQ and control samples, respectively). The oligodendrocyte marker *Hapln2* (adjusted $P = 2.96 \times 10^{-66}$ and 2.18×10^{-79} in MNPQ and control samples, respectively) promotes α-synuclein aggregation and may contribute to neurodegeneration in PD [46,47].

C1qc, which encodes complement subcomponent C1q, was specifically expressed in microglia (adjusted $P = 3.09 \times 10^{-75}$ and 4.82×10^{-87} in MNPQ and control samples, respectively). A meta-analysis of transcriptome data showed that this gene was more strongly expressed in the substantia nigra of PD patients compared to controls [48]. We also found high expression of *Meig1* in ependymal cells (adjusted $P = 1.08 \times 10^{-42}$ and 5.93×10^{-86} in MNPQ and control samples, respectively). The *Meig1* protein binds to the protein encoded by *Pacrg*, a gene co-regulated with *Parkin* [49].

Cldn5 is essential for blood–brain barrier (BBB) integrity [50] and we found that this gene was differentially expressed in endothelial cells (adjusted $P = 2.69 \times 10^{-76}$ and 3.38×10^{-88} in MNPQ and control samples, respectively). Previous work has shown breakdown of the BBB in various neurological disorders, including PD [51].

3.6 Functional enrichment of clusters

The top 10 marker genes showing the highest specificity in each cluster based on minimum P values were used to perform gene set enrichment analysis (GSEA) for biological process using g:Profiler (all adjusted P <0.05; Table S3) [52,53]. Neurons revealed significant enrichments in calcium ion-regulated exocytosis of neurotransmitter, synaptic vesicle fusion to presynaptic active zone membrane, synaptic vesicle exocytosis, signal release from synapse, and neurotransmitter secretion.

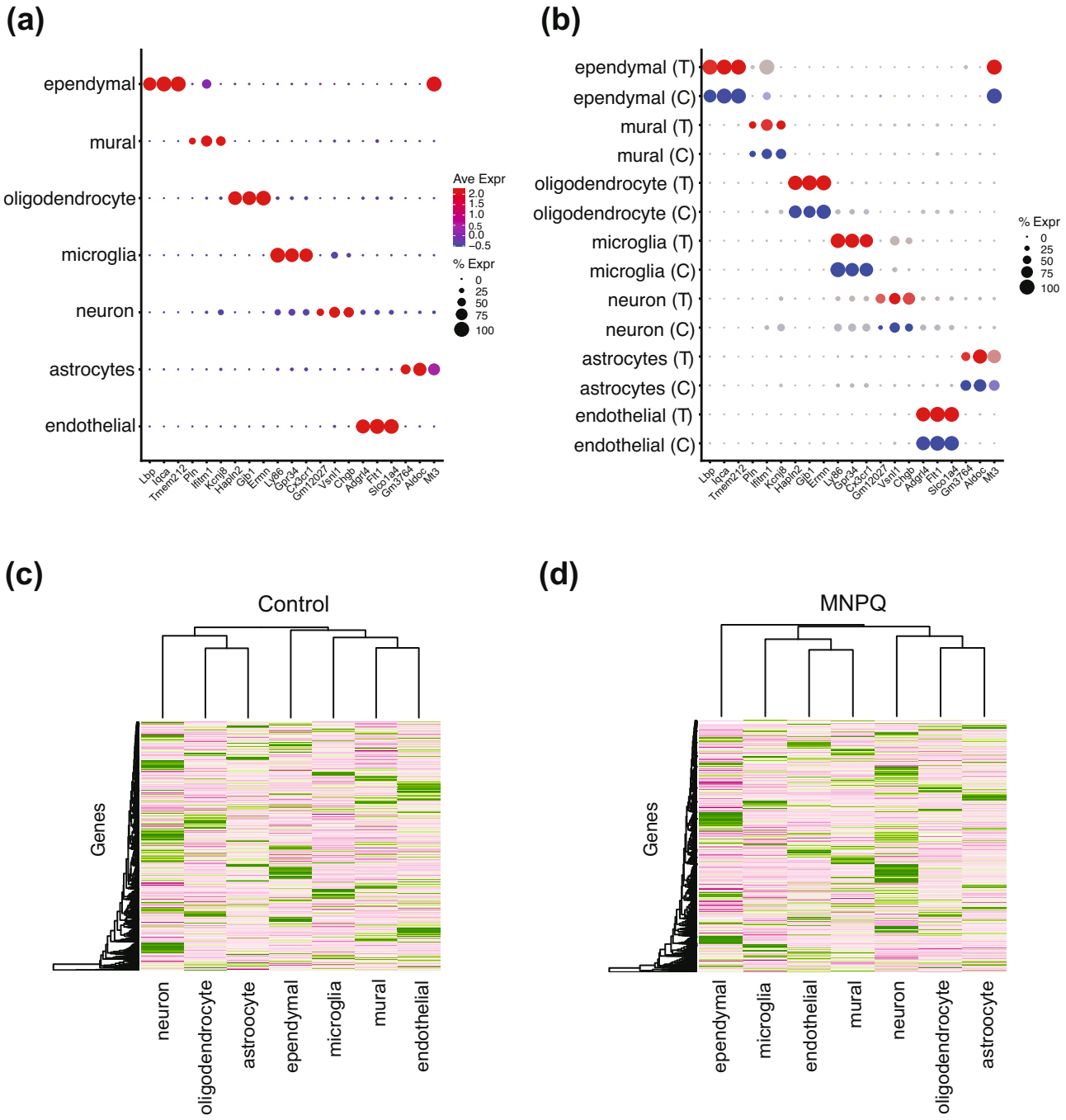

Figure 3: Marker genes for each cell cluster. (a) Marker genes for combined MNPQ and control samples. Average expression (Ave Expr) denoted by red–blue color scale. Percent of cells expressing gene (% Expr) denoted by dot size. (b) Same marker genes separated by sample type; MNPQ treated (T, red–grey expression scale) and control (C, blue–grey expression scale). (c) Heatmap for the average expression of all control markers. (d) MNPQ samples. Cluster specific marker expression apparent.

GSEA of biological process in astrocytes showed significant enrichment in positive regulation of neurofibrillary tangle assembly, inclusion body assembly, and low-density lipoprotein particle remodeling, together with negative regulation of amyloid fibril formation. These biological processes are involved in Alzheimer's disease, which has mechanistic overlaps with PD [54]. In oligodendrocytes, enrichment was observed in the ensheathment of neurons and axon, central nervous system myelination, oligodendrocyte differentiation, and glial cell development.

GSEA of molecular function in neurons showed enrichment in syntaxin binding, SNARE binding, and metal ion

transmembrane transporter activity (Table S3). Astrocytes showed enrichment in low-density lipoprotein particle receptor binding and tau protein binding.

3.7 Expression differences between MNPQ and control mice

Genes with strong cluster-specific expression and large expression differences between MNPQ and vehicle mice were identified (Figures S2–S4 and Table S4). Relatively cluster enriched genes that showed large differences between MNPQ and control included *Dusp3*, *Pianp* (neurons), *Ppp1r3g*, *Tagln3* (astrocytes), and *Glul*, *Bsg* (oligodendrocytes). Some had known links to PD, including *Acp2*, *Rac1*, *Sgta* (neurons) and *Cntfr*, *Fabp5* (astrocytes) [55–59].

In addition to cluster-specific differential expression of genes, there were suggestions of cluster agnostic differential expression. For example, *Gm42418* was strongly downregulated in MNPQ compared to vehicle in all seven cell types. *Gm42418* is a lncRNA and the role of these enigmatic transcripts in brain function, and in neurological disorders such as PD, is becoming more widely appreciated [60,61]. Other differentially expressed genes shared between at least two cell types included *Actb*, *Acls3*, *Agt*, *Atp1b1*, *Btbd17*, *Camk2n1*, *Cmbl*, *Dbp*, *Fabp5*, *Fam23b*, *Id4*, *Igfbp2*, *Malat1*, *Mt2*, *mt-Nd4l*, *Nnat*, *Ndufb5*, *Nap1l3*, *Prpf4b*, *Rgs22*, *Rps26*, *Rpl28*, *Slc6a11*, and *Tagln*. *Malat1* was downregulated by MNPQ in astrocytes and endothelial cells and is a lncRNA that appears to play a role in PD and other neurodegenerative disorders [62].

3.8 Significant differential expression between MNPQ and control samples

P values for differential expression between MNPQ and controls in each cluster were evaluated. All cell clusters, except ependymal cells, had genes whose expression was significantly different between control and sample, giving a total of 1,750 significant genes (Bonferroni adjusted $P < 0.05$) (Table S5). Most genes were expressed at higher levels in the controls; less than one-fifth (304) of the 1,750 significant markers were upregulated in the MNPQ samples. The top three most significant genes in each cell type were *Fam241b*, *Nlk*, *Ss18l1* (astrocyte), *Emx2os*, *Tro*, *Ppip5k1* (endothelial cells), *Bivm*, *Cntrob*, *Nkrf* (microglia), *Gm1439*, *Samd15*, *Pdia5* (mural cells), *Prdm15*, *Sema3e*, *Capn15* (neuron), and *Rai2*, *Dcbld1*, *Entpd7* (oligodendrocyte) (adjusted $P < 1.81 \times 10^{-9}$).

Among the statistically significant genes, 17 overlapped with genes for PD identified from genome-wide association studies ($P < 5 \times 10^{-8}$) [63]. These genes included *Fyn*, *Gak*, *Rit2*, and *Dgkq*. One gene, *Lrrk2*, is also implicated in monogenic PD. Neurons had the largest number of significant genes (472) followed by astrocytes (365), oligodendrocytes (266), endothelial cells (224), microglia (218), and mural cells (211). Our finding of abundant differentially expressed genes in astrocytes is consistent with the finding that this cell type plays an active role in dopaminergic signaling [64]. The significant genes in oligodendrocytes echo a recent scRNA-seq study of normal human substantia nigra suggesting a link between PD risk and these cells [20,22]. Almost one-third of significant differentially expressed genes were shared between two or more clusters. A total of 14 genes, including *Epm2a*, *Sgtb*, *9330182L06Rik*, and *Fam160b2*, overlapped in four or more clusters.

Genes with statistically significant differences in expression between MNPQ and vehicle in each cell type were illustrated in feature plots (Figure S5). Selected genes in each cell type are shown in Figure 4a. Although MNPQ causes decreased average expression of most genes compared to vehicle, the percentage of cells with detectable expression was increased. Figure 4b and c shows heatmaps of the percent of cells expressing genes for all genes and for statistically significant differentially expressed genes. The increased numbers of cells expressing statistically significant but down-regulated genes in the MNPQ samples are apparent.

The increased percentage of expressing cells in the MNPQ mice may represent compensatory induction of low levels of gene expression in normally non-expressing cells. Alternatively, the increased percentage may be an indirect consequence of pesticide-induced cell death selectively destroying non-expressing cells, while sparing any remaining cells with low expression. The genes with low expression may therefore represent a signature of increased cellular resilience to MNPQ.

3.9 Enrichment analysis of significant differentially expressed genes

To identify ubiquitous pathways independent of cell type that play a role in pesticide-induced PD, all 1,750

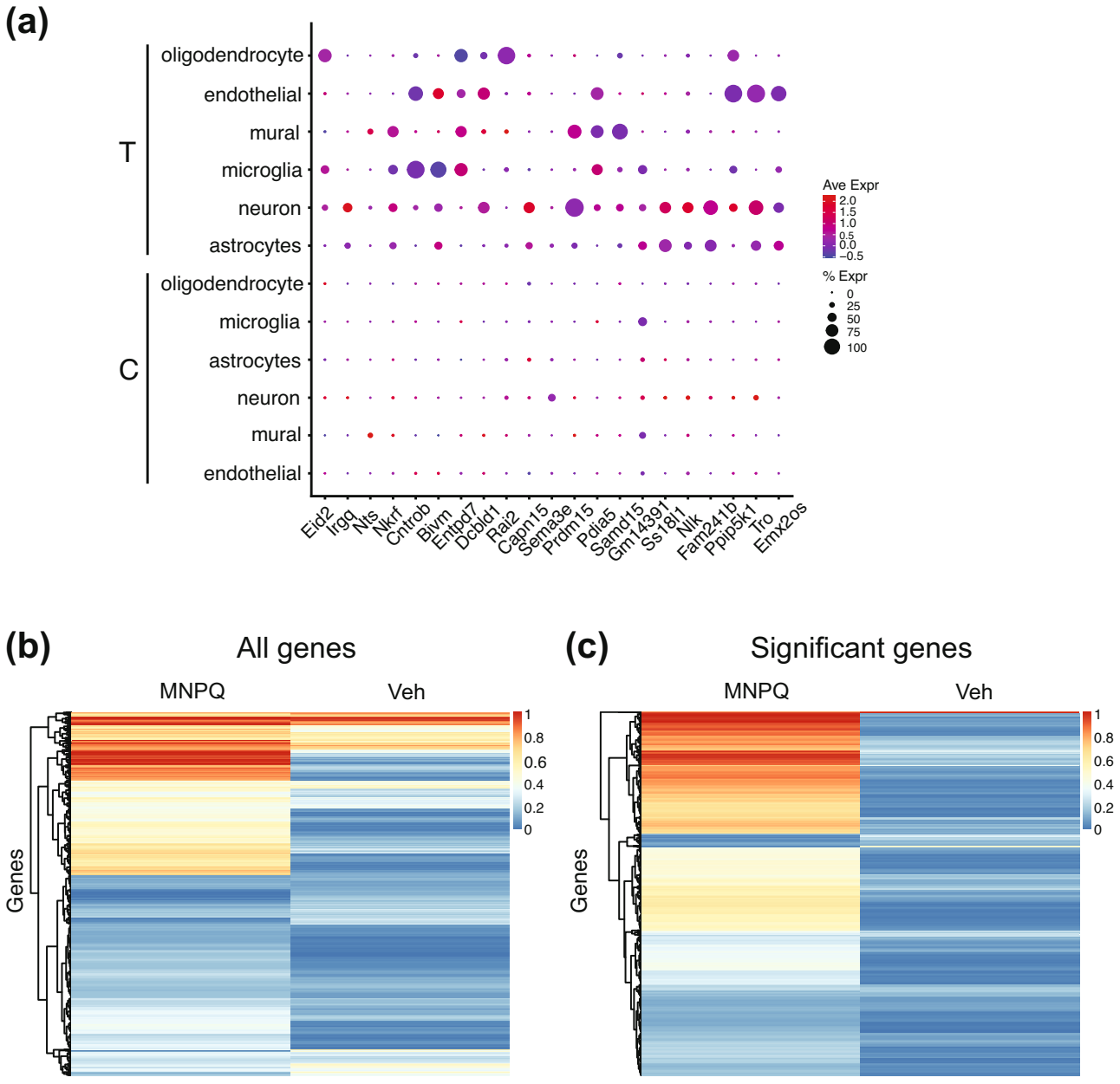

Figure 4: Significant differences in expression between MNPQ and vehicle samples. (a) Significant differences in expression between MNPQ and vehicle in each cell type. Expression is generally lower in the treated (T) samples (blue color) compared to controls (C), even though treated samples have higher percentages of expressing cells. Average expression (Ave Expr) denoted by red–blue color scale. Percent of cells expressing gene (% Expr) denoted by dot size. (b) Heatmap of percent of cells using all genes from all clusters. Increased cell percentage expressing genes in MNPQ compared to vehicle. (c) Heatmap of cell percentage for statistically significant genes.

significant differentially expressed genes in the SNpc were analyzed for functional enrichment (Table S6). Functions relevant to PD were found to be over-represented using gene ontology (GO) in Enrichr, including regulation of axonogenesis, modulation of chemical synaptic transmission, neuron projection morphogenesis, and regulation of AMPA receptor activity (adjusted $P < 4.7 \times 10^{-7}$) [65,66].

We also evaluated KEGG pathways in the significant differentially expressed genes [67] (Table S6). Pathways were enriched in terms relevant to PD, such as GABAergic synapse pathway, dopaminergic synapse and cholinergic synapse (adjusted $P < 9.4 \times 10^{-4}$). Relevant genes included *Prkacb*, *Fos*, *Adcy5*, and *Homer1* [68–71].

The significant differentially expressed genes were also strongly enriched in terms related to PD in the

GeneRIF ARCHS4 predictions of rare diseases [72,73]. These terms included dystonia, neuronal intranuclear inclusion disease, and PD juvenile autosomal recessive (adjusted $P < 3.03 \times 10^{-24}$). Consistent with the increased risk of PD in older individuals, the significant differentially expressed genes were enriched in downregulated gene expression signatures in the GTEx catalog of aging human brain (20–29 vs 60–69 years, adjusted $P = 1.64 \times 10^{-10}$) [74].

3.10 Networks of significant differentially expressed genes

To further dissect genetic pathways in pesticide-induced PD, we used GeneMANIA to analyze the top 100 most significant differentially expressed genes between MNPQ and vehicle-treated mice in neurons (Figure 5). GeneMANIA generates hypotheses about gene function by identifying networks of genes with similar roles based on publicly available genomics and proteomics data [75].

The most common interactions in the network were due to genetic interactions inferred from radiation hybrid genotypes [76]. These interactions composed half of the total and were six times more common than the next most frequent, which were from the InterPro classification of protein families [77]. The network was significantly enriched in terms solely related to collagen, extracellular matrix, and basement membrane (FDR $< 8.49 \times 10^{-4}$) even though constructed using differentially expressed genes in neurons, suggesting a surprising connection between neurodegeneration and the extracellular matrix (Figure 5a). Other studies have also implicated changes in the extracellular matrix as a result of PD [78–80]. One hub gene, *Cacna1c*, had 31 interactions (Figure 5b). L-type calcium channels, such as *Cacna1c*, are implicated in PD, and pharmacological blockade of these channels has been proposed as a potential therapy for the disorder [81–83].

We extended our analysis by using all significant differentially expressed genes to create a network of protein–protein interactions from the InnateDB tool in OmicsNet [84,85]. InnateDB curates extensive experimentally validated molecular interactions and pathway annotations for both human and mouse. We found that *Nova1* acted as hub gene with 115 linked nodes among the significant differentially expressed genes in all clusters (Figure S6). *Nova1* was significantly more highly expressed in MNPQ neurons than controls (adjusted $P = 1.03 \times 10^{-4}$). Interestingly, *Nova1* regulates neuron-

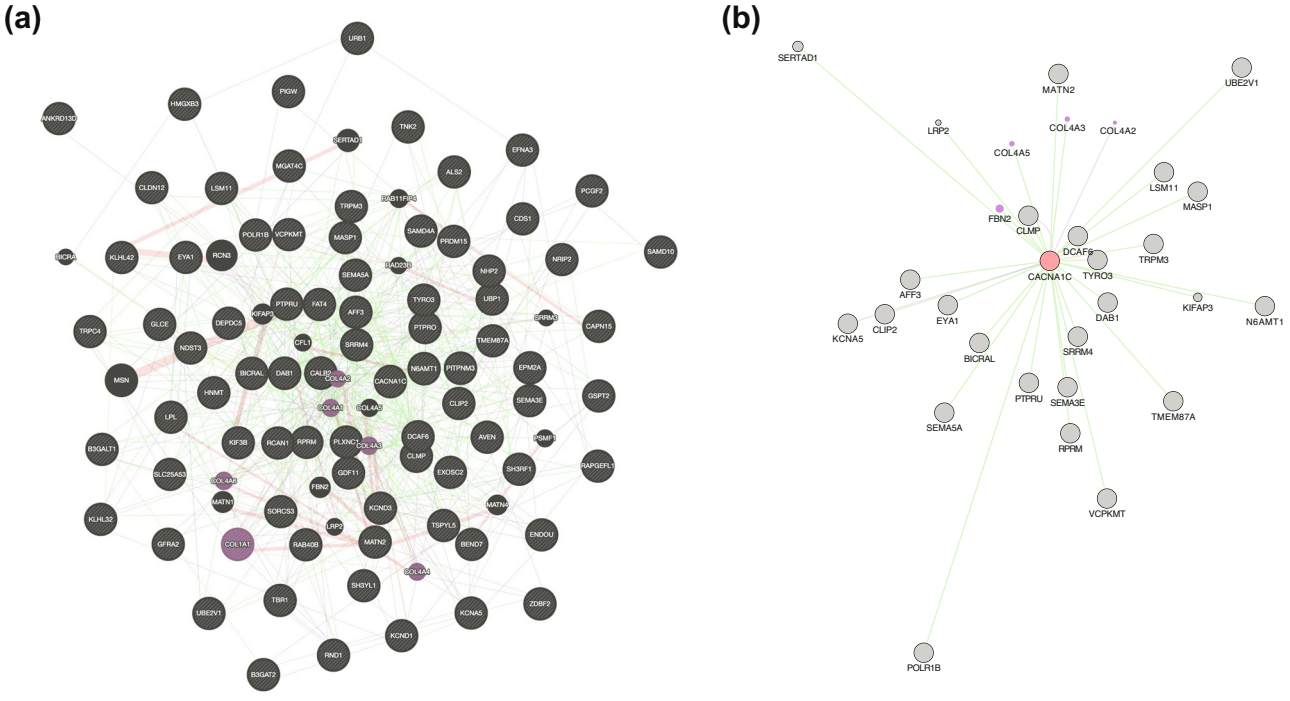

Figure 5: Networks for significant differentially expressed genes in neurons. (a) The network is significantly enriched in extracellular matrix genes (purple). The most common interactions are genetic interactions from radiation hybrid genotypes (green). (b) Subnetwork featuring Cacna1c.

specific alternative splicing and also binds to a *cis*-regulatory region in the α-synuclein gene, which is linked to PD via both common and rare variants [86,87].

4 Discussion

4.1 Mouse model of pesticide-induced PD

To model pesticide-induced PD, we treated C57BL/6J mice with MNPQ or vehicle. Motor effects reminiscent of PD were detected in the MNPQ-treated mice using the pole test. We used scRNA-seq of the SNpc of MNPQ and control mice to understand the molecular signatures of pesticide-induced PD at a cellular level.

We chose combined dosing with MNPQ for a number of reasons [88]. Individually, both MN and PQ cause dopaminergic neurodegeneration and motor impairment in mice. However, when administered together, these agents cause a more severe neurodegeneration and PD phenotype. The MNPQ model is lent further credence by the fact that MN and PQ are frequently employed in the same locales and workers exposed to both agents show an elevated risk of PD.

We followed a published regimen for the administration of MNPQ in mice, in which the pesticides were given by i.p. injection [14,15]. Six doses are required for an effective model of PD in the C57BL/6J background (Marie-Françoise Chesselet, unpublished observations). In addition, spaced administration of the pesticides was used to minimize animal loss. The duration of pesticide exposure feasible in an animal model is much more limited than for agricultural workers over the course of their careers. To render an effective mouse model, peak MNPQ concentrations thousands of times higher than typically found in humans are hence required [89–91].

The SNpc was punch dissected based on its anatomical location. Contamination with the substantia nigra pars reticulata (SNpr) is possible and may affect our results. Nevertheless, since the major changes in PD are found in the SNpc, contamination by SNpr cells would likely decrease the significance of our findings rather than causing false-positive results.

Loss of tyrosine hydroxylase/dopaminergic (TH/DA) neurons can show inter-study variability in mouse models of PD. While we did not verify the loss of TH/DA neurons using immunohistochemistry, we found behavioral deficits reminiscent of PD, which are consistent with the loss of these neurons. In addition, functional enrichment of the scRNA-seq data is highly consistent with the loss of TH/DA neurons, suggesting correct implementation of our pesticide-induced mouse model of PD.

4.2 scRNA-seq

We expected to capture >10,000 single cells expressing the transcriptome from most mouse genes. Indeed, using initial filtering conditions, we obtained the expression of transcripts from 11,252 to 10,287 cells for control and experimental samples, respectively, which met our expectations [92,93]. However, when we used stringent filtering criteria to remove dead cells and ambient RNA from the data, only 494 and 468 single cells remained for evaluation. This number of cells is less than ideal, but we decided that exploratory analysis of these pilot data may give some insights into the cellular and molecular mechanisms of pesticide-induced PD.

Unsupervised clustering gave 13 groups at first. However, employing marker genes to assign clusters to specific cell types resulted in a total of seven clusters. The majority of markers in each cluster were specific except for a few that overlapped between clusters. The overlapping markers may be due to proliferating precursor cells that share transcriptional profiles, even though they are destined to form different cell types [94].

Genes were identified in each cluster with increased expression relevant to dopaminergic neurotransmission and pesticide-induced PD. Examples of cluster-specific genes included neuron (*Syt1*, *Snap25*, and *Rtn1*), astrocyte (*Gpr37l1*, *Pla2g7*, and *Prdx6*), and oligodendrocytes (*Ermn*, *Cldn11*, and *Ugt8a*).

Despite the small number of isolated cells, 1,750 genes were identified with statistically significant up- and down-regulation between MNPQ and controls. Significant differentially expressed genes were found in all cell clusters, except ependymal. The lack of differentially expressed genes in ependymal cells may reflect either the modest recovery of viable cells in our study or possibly the unimportance of ependymal cells in pesticide-induced PD.

The significantly differentially expressed genes showed some commonality with PD genes identified using genome-wide association, with one gene, *Lrrk2*, also responsible for monogenic PD. The largest number of significant differentially expressed genes was found in neurons, followed by astrocytes and oligodendrocytes. This finding demonstrates that not only neurons but also support cells play a role in the pathogenesis of pesticide-induced PD.

A total of 14 genes were significantly differentially expressed in four or more cell types in the SNpc, suggesting that cell-agnostic as well as cell-specific pathways play a role in pesticide-induced PD. Functional enrichment analysis of differentially expressed genes using GO highlighted processes relevant to PD, such as regulation of axonogenesis, modulation of chemical synaptic transmission, neuron projection morphogenesis, and regulation of AMPA receptor activity. In addition, KEGG pathways included GABAergic synapse pathway, dopaminergic synapse, and cholinergic synapse.

In a literature database of rare diseases, the significant differentially expressed genes were strongly enriched in terms related to neuronal intranuclear inclusion disease and juvenile PD, highlighting the relationships between pesticide-induced and other causes of PD. The significant differentially expressed genes were also enriched in terms related to gene expression signatures in aging human brain, consistent with PD as mostly a disease of older people.

We performed a network analysis of 100 significant differentially expressed genes in neurons using GeneMANIA. In addition to the canonical PD pathways discussed above, this network underlined the importance of the interface between neurons and the extracellular matrix in pesticide-induced PD. This finding, together with the relevance of astrocytes and oligodendrocytes, further emphasizes that PD is not solely a disorder of neurons. Network analysis of all differentially expressed genes using InnateDB indicated that *Nova1*, a regulator of alternative splicing, acts as a hub gene and is expressed at higher levels in MNPQ SNpc neurons than controls. This observation draws attention to *Nova1* as a key regulator in PD.

5 Conclusion

Employing a model of pesticide-induced PD in mice, together with scRNA-seq analysis, we were able to classify different cell types in the SNpc and delineate significant expression differences between pesticide-exposed and control cells. Gene enrichment and network analyses of differentially expressed genes highlighted relevant genetic pathways in the model.

Clinical trials have so far demonstrated limited, if any, success in slowing PD progression. Nevertheless, multiple cell-specific genetic pathways appear to converge onto the final common conduit of dopaminergic neurodegeneration in PD. Single-cell analysis may allow development of more highly targeted therapies that improve therapeutic outcomes and minimize side effects. Thus, further studies using scRNA-seq will help dissect the environmental and genetic risk factors that cause pesticide-induced PD, while pointing toward novel strategies for intervention.

Acknowledgments: We thank the UCLA Semel Institute Neurosciences Genomics Core for sequencing.

Funding information: We thank the American PD Association Center for Advanced Research (Marie-Françoise Chesselet, Beate Ritz, Principal Investigators) for funding.

Author contributions: A.H.K. and L.K.L.: acquisition of data, analysis and interpretation of data, and drafting or revising the article. D.J.S.: conception and design, analysis and interpretation of data, and drafting or revising the article.

Conflict of interest: Authors state no conflict of interest.

Data availability statement: The sequencing data generated in this study can be downloaded from the NCBI BioProject database (https://www.ncbi.nlm.nih.gov/bioproject/) under accession number PRJNA756542. Supplementary figures, tables, and data are also freely available from figshare (https://figshare.com/; doi:10.6084/m9.figshare.19197056).

References

[1] Kalia LV, Lang AE. Parkinson's disease. Lancet. 2015;386:896–912. doi: 10.1016/S0140-6736(14)61393-3.
[2] Fahn S, Sulzer D. Neurodegeneration and neuroprotection in Parkinson disease. Neurotherapeutics. 2004;1:139–54. doi: 10.1602/neurorx.1.1.139.
[3] Zhong J, Tang G, Zhu J, Wu W, Li G, Lin X, et al. Single-cell brain atlas of Parkinson's disease mouse model. J Genet Genomics. 2021;48:277–88. doi: 10.1016/j.jgg.2021.01.003.
[4] Fernagut PO, Hutson CB, Fleming SM, Tetreaut NA, Salcedo J, Masliah E, et al. Behavioral and histopathological consequences of paraquat intoxication in mice: Effects of α-synuclein over-expression. Synapse. 2007;61:991–1001. doi: 10.1002/syn.20456.
[5] Nalls MA, Blauwendraat C, Vallerga CL, Heilbron K, Bandres-Ciga S, Chang D, et al. Identification of novel risk loci, causal insights, and heritable risk for Parkinson's disease: a meta-analysis of genome-wide association studies. Lancet Neurol. 2019;18:1091–102. doi: 10.1016/S1474-4422(19)30320-5.
[6] Blauwendraat C, Nalls MA, Singleton AB. The genetic architecture of Parkinson's disease. Lancet Neurol. 2020;19:170–8. doi: 10.1016/S1474-4422(19)30287-X.

[7] Chambers-Richards T, Su Y, Chireh B, D'Arcy C. Exposure to toxic occupations and their association with Parkinson's disease: a systematic review with meta-analysis. Rev Env Health. 2021. Online ahead of print. doi: 10.1515/reveh-2021-0111.
[8] Hatcher J, Pennell K, Miller G. Parkinson's disease and pesticides: a toxicological perspective. Trends Pharmacol Sci. 2008;29:322–9. doi: 10.1016/j.tips.2008.03.007.
[9] Ascherio A, Chen H, Weisskopf MG, O'reilly E, McCullough ML, Calle EE, et al. Pesticide exposure and risk for Parkinson's disease. Ann Neurol. 2006;60:197–203. doi: 10.1002/ana.20904.
[10] Wang A, Costello S, Cockburn M, Zhang X, Bronstein J, Ritz B. Parkinson's disease risk from ambient exposure to pesticides. Eur J Epidemiol. 2011;26:547–55. doi: 10.1007/s10654-011-9574-5.
[11] Chin MH, Qian W-J, Wang H, Petyuk VA, Bloom JS, Sforza DM, et al. Mitochondrial dysfunction, oxidative stress, and apoptosis revealed by proteomic and transcriptomic analyses of the striata in two mouse models of Parkinson's disease. J Proteome Res. 2008;7:666–77. doi: 10.1021/pr070546l.
[12] Helley MP, Pinnell J, Sportelli C, Tieu K. Mitochondria: A common target for genetic mutations and environmental toxicants in Parkinson's disease. Front Genet. 2017;8:177. doi: 10.3389/fgene.2017.00177.
[13] Smith DJ. Mitochondrial dysfunction in mouse models of Parkinson's disease revealed by transcriptomics and proteomics. J Bioenerg Biomembr. 2009;41:487–91. doi: 10.1007/s10863-009-9254-2.
[14] Gollamudi S, Johri A, Calingasan NY, Yang L, Elemento O, Beal MF. Concordant signaling pathways produced by pesticide exposure in mice correspond to pathways identified in human Parkinson's disease. PLoS ONE. 2012;7:e36191. doi: 10.1371/journal.pone.0036191.
[15] Richter F, Gabby L, McDowell KA, Mulligan CK, De La Rosa K, Sioshansi PC, et al. Effects of decreased dopamine transporter levels on nigrostriatal neurons and paraquat/maneb toxicity in mice. Neurobiol Aging. 2017;51:54–66. doi: 10.1016/j.neurobiolaging.2016.11.015.
[16] Borrageiro G, Haylett W, Seedat S, Kuivaniemi H, Bardien S. A review of genome-wide transcriptomics studies in Parkinson's disease. Eur J Neurosci. 2018;47:1–16. doi: 10.1111/ejn.13760.
[17] Brown VM, Ossadtchi A, Khan AH, Yee S, Lacan G, Melega WP, et al. Multiplex three-dimensional brain gene expression mapping in a mouse model of Parkinson's disease. Genome Res. 2002;12:868–84. doi: 10.1101/gr.229002.
[18] Greene JG. Current status and future directions of gene expression profiling in Parkinson's disease. Neurobiol Dis. 2012;45:76–82. doi: 10.1016/j.nbd.2010.10.022.
[19] Ma S-X, Lim SB. Single-cell RNA sequencing in Parkinson's disease. Biomedicines. 2021;9:368. doi: 10.3390/biomedicines9040368.
[20] Agarwal D, Sandor C, Volpato V, Caffrey TM, Monzón-Sandoval J, Bowden R, et al. A single-cell atlas of the human substantia nigra reveals cell-specific pathways associated with neurological disorders. Nat Commun. 2020;11:4183. doi: 10.1038/s41467-020-17876-0.
[21] Bryois J, Skene NG, Hansen TF, Kogelman LJA, Watson HJ, Liu Z, et al. Genetic identification of cell types underlying brain complex traits yields insights into the etiology of Parkinson's disease. Nat Genet. 2020;52:482–93. doi: 10.1038/s41588-020-0610-9.
[22] Errea O, Rodriguez-Oroz MC. Oligodendrocytes, a new player in the etiology of Parkinson's disease. Mov Disord. 2021;36:83–3. doi: 10.1002/mds.28393.
[23] Skene NG, Grant SGN. Identification of vulnerable cell types in major brain disorders using single cell transcriptomes and expression weighted cell type enrichment. Front Neurosci. 2016;10:16. doi: 10.3389/fnins.2016.00016.
[24] Lang C, Campbell KR, Ryan BJ, Carling P, Attar M, Vowles J, et al. Single-cell sequencing of iPSC-dopamine neurons reconstructs disease progression and identifies HDAC4 as a regulator of parkinson cell phenotypes. Cell Stem Cell. 2019;24:93–106.e6. doi: 10.1016/j.stem.2018.10.023.
[25] Taylor TN, Caudle WM, Shepherd KR, Noorian A, Jackson CR, Iuvone PM, et al. Nonmotor symptoms of Parkinson's disease revealed in an animal model with reduced monoamine storage capacity. J Neurosci. 2009;29:8103–13. doi: 10.1523/JNEUROSCI.1495-09.2009.
[26] Magen I, Chesselet M-F. Parkinson's disease. In: Pietropaolo S, Sluyter F, Crusio WE, editors. Behavioral Genetics of the Mouse. 1st edn. Cambridge, UK: Cambridge University Press; 2014. p. 411–35. doi: 10.1017/CBO9781107360556.031.
[27] Matsuura K, Kabuto H, Makino H, Ogawa N. Pole test is a useful method for evaluating the mouse movement disorder caused by striatal dopamine depletion. J Neurosci Methods. 1997;73:45–8. doi: 10.1016/S0165-0270(96)02211-X.
[28] Bates D, Mächler M, Bolker B, Walker S. Fitting linear mixed-effects models using lme4. J Stat Soft. 2015;67:1–48. doi: 10.18637/jss.v067.i01.
[29] R Core Team. R: a language and environment for statistical computing; 2022. https://www.R-project.org/.
[30] Lenth RV. emmeans: estimated marginal means, aka least-squares means; 2022. https://CRAN.R-project.org/package = emmeans.
[31] Hao Y, Hao S, Andersen-Nissen E, Mauck WM, Zheng S, Butler A, et al. Integrated analysis of multimodal single-cell data. Cell. 2021;184:3573–87.e29. doi: 10.1016/j.cell.2021.04.048.
[32] Achim K, Pettit J-B, Saraiva LR, Gavriouchkina D, Larsson T, Arendt D, et al. High-throughput spatial mapping of single-cell RNA-seq data to tissue of origin. Nat Biotechnol. 2015;33:503–9. doi: 10.1038/nbt.3209.
[33] Macosko EZ, Basu A, Satija R, Nemesh J, Shekhar K, Goldman M, et al. Highly parallel genome-wide expression profiling of individual cells using nanoliter droplets. Cell. 2015;161:1202–14. doi: 10.1016/j.cell.2015.05.002.
[34] McGinnis CS, Murrow LM, Gartner ZJ. DoubletFinder: Doublet detection in single-cell RNA sequencing data using artificial nearest neighbors. Cell Syst. 2019;8:329–37.e4. doi: 10.1016/j.cels.2019.03.003.
[35] Shalek AK, Satija R, Adiconis X, Gertner RS, Gaublomme JT, Raychowdhury R, et al. Single-cell transcriptomics reveals bimodality in expression and splicing in immune cells. Nature. 2013;498:236–40. doi: 10.1038/nature12172.
[36] Zhang X, Lan Y, Xu J, Quan F, Zhao E, Deng C, et al. CellMarker: a manually curated resource of cell markers in human and mouse. Nucleic Acids Res. 2019;47:D721–8. doi: 10.1093/nar/gky900.

[37] Noor A, Zahid S. A review of the role of synaptosomal-associated protein 25 (SNAP-25) in neurological disorders. Int J Neurosci. 2017;127:805–11. doi: 10.1080/00207454.2016.1248240.
[38] Chang J, Zhang X-L, Yu H, Chen J. Downregulation of RTN1-C attenuates MPP + -induced neuronal injury through inhibition of mGluR5 pathway in SN4741 cells. Brain Res Bull. 2019;146:1–6. doi: 10.1016/j.brainresbull.2018.11.026.
[39] Bai X, Strong R. Expression of synaptophysin protein in different dopaminergic cell lines. J Biochem Pharmacol Res. 2014;2:185–90.
[40] Hertz E, Terenius L, Vukojević V, Svenningsson P. GPR37 and GPR37L1 differently interact with dopamine 2 receptors in live cells. Neuropharmacology. 2019;152:51–7. doi: 10.1016/j.neuropharm.2018.11.009.
[41] Morató X, Garcia-Esparcia P, Argerich J, Llorens F, Zerr I, Paslawski W, et al. Ecto-GPR37: A potential biomarker for Parkinson's disease. Transl Neurodegener. 2021;10:8. doi: 10.1186/s40035-021-00232-7.
[42] Zhu J, Sun T, Zhang J, Liu Y, Wang D, Zhu H, et al. Drd2 biased agonist prevents neurodegeneration against NLRP3 inflammasome in Parkinson's disease model via a β-arrestin2-biased mechanism. Brain Behav Immun. 2020;90:259–71. doi: 10.1016/j.bbi.2020.08.025.
[43] Imai Y, Soda M, Inoue H, Hattori N, Mizuno Y, Takahashi R. An unfolded putative transmembrane polypeptide, which can lead to endoplasmic reticulum stress, is a substrate of parkin. Cell. 2001;105:891–902. doi: 10.1016/S0092-8674(01)00407-X.
[44] Magrinelli F, Mehta S, Di Lazzaro G, Latorre A, Edwards MJ, Balint B, et al. Dissecting the phenotype and genotype of *PLA2G6*-related parkinsonism. Mov Disord. 2021;37:148–61. doi: 10.1002/mds.28807.
[45] Yun H-M, Choi DY, Oh KW, Hong JT. PRDX6 exacerbates dopaminergic neurodegeneration in a MPTP mouse model of Parkinson's disease. Mol Neurobiol. 2015;52:422–31. doi: 10.1007/s12035-014-8885-4.
[46] Wang Q, Zhou Q, Zhang S, Shao W, Yin Y, Li Y, et al. Elevated Hapln2 expression contributes to protein aggregation and neurodegeneration in an animal model of Parkinson's disease. Front Aging Neurosci. 2016;8:197. doi: 10.3389/fnagi.2016.00197.
[47] Wang Q, Wang C, Ji B, Zhou J, Yang C, Chen J. Hapln2 in neurological diseases and its potential as therapeutic target. Front Aging Neurosci. 2019;11:60. doi: 10.3389/fnagi.2019.00060.
[48] Mariani E, Frabetti F, Tarozzi A, Pelleri MC, Pizzetti F, Casadei R. Meta-analysis of Parkinson's disease transcriptome data using TRAM software: Whole substantia nigra tissue and single dopamine neuron differential gene expression. PLoS ONE. 2016;11:e0161567. doi: 10.1371/journal.pone.0161567.
[49] Khan N, Pelletier D, McAlear TS, Croteau N, Veyron S, Bayne AN, et al. Crystal structure of human PACRG in complex with MEIG1 reveals roles in axoneme formation and tubulin binding. Structure. 2021;29:572–86.e6. doi: 10.1016/j.str.2021.01.001.
[50] Ahn J-C, Hwang SJ, Lee H-J, Kim K-W. Claudin-5a knockdown attenuates blood-neural barrier in zebrafish. Comp Biochem Physiol C Toxicol Pharmacol. 2021;250:109176. doi: 10.1016/j.cbpc.2021.109176.
[51] Obermeier B, Daneman R, Ransohoff RM. Development, maintenance and disruption of the blood-brain barrier. Nat Med. 2013;19:1584–96. doi: 10.1038/nm.3407.
[52] Raudvere U, Kolberg L, Kuzmin I, Arak T, Adler P, Peterson H, et al. g:Profiler: a web server for functional enrichment analysis and conversions of gene lists (2019 update). Nucleic Acids Res. 2019;47:W191–8. doi: 10.1093/nar/gkz369.
[53] Subramanian A, Tamayo P, Mootha VK, Mukherjee S, Ebert BL, Gillette MA, et al. Gene set enrichment analysis: A knowledge-based approach for interpreting genome-wide expression profiles. Proc Natl Acad Sci USA. 2005;102:15545–50. doi: 10.1073/pnas.0506580102.
[54] Wakasugi N, Hanakawa T. It is time to study overlapping molecular and circuit pathophysiologies in Alzheimer's and lewy body disease spectra. Front Syst Neurosci. 2021;15:777706. doi: 10.3389/fnsys.2021.777706.
[55] Ashtari N, Jiao X, Rahimi-Balaei M, Amiri S, Mehr SE, Yeganeh B, et al. Lysosomal acid phosphatase biosynthesis and dysfunction: A mini review focused on lysosomal enzyme dysfunction in brain. Curr Mol Med. 2016;16:439–46. doi: 10.2174/1566524016666160429115834.
[56] Guiler W, Koehler A, Boykin C, Lu Q. Pharmacological modulators of small GTPases of rho family in neurodegenerative diseases. Front Cell Neurosci. 2021;15:661612. doi: 10.3389/fncel.2021.661612.
[57] Kubota S, Doi H, Koyano S, Tanaka K, Komiya H, Katsumoto A, et al. SGTA associates with intracellular aggregates in neurodegenerative diseases. Mol Brain. 2021;14:59. doi: 10.1186/s13041-021-00770-1.
[58] Pöyhönen S, Er S, Domanskyi A, Airavaara M. Effects of neurotrophic factors in glial cells in the central nervous system: Expression and properties in neurodegeneration and injury. Front Physiol. 2019;10:486. doi: 10.3389/fphys.2019.00486.
[59] Wang Y, Shinoda Y, Cheng A, Kawahata I, Fukunaga K. Epidermal fatty acid-binding Protein 5 (FABP5) involvement in alpha-synuclein-induced mitochondrial injury under oxidative stress. Biomedicines. 2021;9:110. doi: 10.3390/biomedicines9020110.
[60] Andersen RE, Lim DA. Forging our understanding of lncRNAs in the brain. Cell Tissue Res. 2018;371:55–71. doi: 10.1007/s00441-017-2711-z.
[61] Taghizadeh E, Gheibihayat SM, Taheri F, Afshani SM, Farahani N, Saberi A. LncRNAs as putative biomarkers and therapeutic targets for Parkinson's disease. Neurol Sci. 2021;42:4007–15. doi: 10.1007/s10072-021-05408-7.
[62] Lu Y, Gong Z, Jin X, Zhao P, Zhang Y, Wang Z. LncRNA MALAT1 targeting miR-124-3p regulates DAPK1 expression contributes to cell apoptosis in Parkinson's disease. J Cell Biochem. 2020;121:4838–48. doi: 10.1002/jcb.29711.
[63] Buniello A, MacArthur JAL, Cerezo M, Harris LW, Hayhurst J, Malangone C, et al. The NHGRI-EBI GWAS Catalog of published genome-wide association studies, targeted arrays and summary statistics 2019. Nucleic Acids Res. 2019;47:D1005–12. doi: 10.1093/nar/gky1120.
[64] Corkrum M, Covelo A, Lines J, Bellocchio L, Pisansky M, Loke K, et al. Dopamine-evoked synaptic regulation in the nucleus accumbens requires astrocyte activity. Neuron. 2020;105:1036–47.e5. doi: https://doi.org/10.1016/j.neuron.2019.12.026.

[65] Kuleshov MV, Jones MR, Rouillard AD, Fernandez NF, Duan Q, Wang Z, et al. Enrichr: a comprehensive gene set enrichment analysis web server 2016 update. Nucleic Acids Res. 2016;44:W90–7. doi: 10.1093/nar/gkw377.
[66] The Gene Ontology Consortium, Carbon S, Douglass E, Good BM, Unni DR, Harris NL, et al. The gene ontology resource: Enriching a gold mine. Nucleic Acids Res. 2021;49:D325–34. doi: 10.1093/nar/gkaa1113.
[67] Kanehisa M, Araki M, Goto S, Hattori M, Hirakawa M, Itoh M, et al. KEGG for linking genomes to life and the environment. Nucleic Acids Res. 2007;36:D480–4. doi: 10.1093/nar/gkm882.
[68] Erro R, Mencacci NE, Bhatia KP. The emerging role of phosphodiesterases in movement disorders. Mov Disord. 2021;36:2225–43. doi: 10.1002/mds.28686.
[69] Odumpatta R, Arumugam M. Integrative analysis of gene expression and regulatory network interaction data reveals the protein Kinase C family of serine/threonine receptors as a significant druggable target for Parkinson's disease. J Mol Neurosci. 2021;71:466–80. doi: 10.1007/s12031-020-01669-7.
[70] Tran AA, De Smet M, Grant GD, Khoo TK, Pountney DL. Investigating the convergent mechanisms between major depressive disorder and Parkinson's disease. Complex Psychiatry. 2020;6:47–61. doi: 10.1159/000512657.
[71] Zhu M, Cortese GP, Waites CL. Parkinson's disease-linked Parkin mutations impair glutamatergic signaling in hippocampal neurons. BMC Biol. 2018;16:100. doi: 10.1186/s12915-018-0567-7.
[72] Jimeno-Yepes AJ, Sticco JC, Mork JG, Aronson AR. GeneRIF indexing: sentence selection based on machine learning. BMC Bioinforma. 2013;14:171. doi: 10.1186/1471-2105-14-171.
[73] Lachmann A, Torre D, Keenan AB, Jagodnik KM, Lee HJ, Wang L, et al. Massive mining of publicly available RNA-seq data from human and mouse. Nat Commun. 2018;9:1366. doi: 10.1038/s41467-018-03751-6.
[74] The GTEx Consortium. The GTEx Consortium atlas of genetic regulatory effects across human tissues. Science. 2020;369:1318–30. doi: 10.1126/science.aaz1776.
[75] Franz M, Rodriguez H, Lopes C, Zuberi K, Montojo J, Bader GD, et al. GeneMANIA update 2018. Nucleic Acids Res. 2018;46:W60–4. doi: 10.1093/nar/gky311.
[76] Lin A, Wang RT, Ahn S, Park CC, Smith DJ. A genome-wide map of human genetic interactions inferred from radiation hybrid genotypes. Genome Res. 2010;20:1122–32. doi: 10.1101/gr.104216.109.
[77] Blum M, Chang H-Y, Chuguransky S, Grego T, Kandasaamy S, Mitchell A, et al. The InterPro protein families and domains database: 20 years on. Nucleic Acids Res. 2021;49:D344–54. doi: 10.1093/nar/gkaa977.
[78] Aguila J, Cheng S, Kee N, Cao M, Wang M, Deng Q, et al. Spatial RNA sequencing identifies robust markers of vulnerable and resistant human midbrain dopamine neurons and their expression in Parkinson's disease. Front Mol Neurosci. 2021;14:699562. doi: 10.3389/fnmol.2021.699562.
[79] Freitas A, Aroso M, Barros A, Fernández M, Conde-Sousa E, Leite M, et al. Characterization of the striatal extracellular matrix in a mouse model of Parkinson's disease. Antioxidants. 2021;10:1095. doi: 10.3390/antiox10071095.
[80] Sandor C, Honti F, Haerty W, Szewczyk-Krolikowski K, Tomlinson P, Evetts S, et al. Whole-exome sequencing of 228 patients with sporadic Parkinson's disease. Sci Rep. 2017;7:41188. doi: 10.1038/srep41188.
[81] Kasap M, Dwyer DS. Na + leak-current channel (NALCN) at the junction of motor and neuropsychiatric symptoms in Parkinson's disease. J Neural Transm. 2021;128:749–62. doi: 10.1007/s00702-021-02348-6.
[82] Liss B, Striessnig J. The potential of L-type calcium channels as a drug target for neuroprotective therapy in Parkinson's disease. Annu Rev Pharmacol Toxicol. 2019;59:263–89. doi: 10.1146/annurev-pharmtox-010818-021214.
[83] Ritz B, Rhodes SL, Qian L, Schernhammer E, Olsen JH, Friis S. L-type calcium channel blockers and Parkinson disease in denmark. Ann Neurol. 2010;67:600–6. doi: 10.1002/ana.21937.
[84] Breuer K, Foroushani AK, Laird MR, Chen C, Sribnaia A, Lo R, et al. InnateDB: systems biology of innate immunity and beyond–recent updates and continuing curation. Nucleic Acids Res. 2013;41:D1228–33. doi: 10.1093/nar/gks1147.
[85] Zhou G, Xia J. Using OmicsNet for network integration and 3D visualization. Curr Protoc Bioinforma. 2019;65:e69. doi: 10.1002/cpbi.69.
[86] Jensen KB, Dredge BK, Stefani G, Zhong R, Buckanovich RJ, Okano HJ, et al. Nova-1 regulates neuron-specific alternative splicing and is essential for neuronal viability. Neuron. 2000;25:359–71. doi: 10.1016/S0896-6273(00)80900-9.
[87] McClymont SA, Hook PW, Soto AI, Reed X, Law WD, Kerans SJ, et al. Parkinson-associated SNCA enhancer variants revealed by open chromatin in mouse dopamine neurons. Am J Hum Genet. 2018;103:874–92. doi: 10.1016/j.ajhg.2018.10.018.
[88] Colle D, Santos DB, Naime AA, Gonçalves CL, Ghizoni H, Hort MA, et al. Early postnatal exposure to paraquat and maneb in mice increases nigrostriatal dopaminergic susceptibility to a Re-challenge with the same pesticides at adulthood: Implications for Parkinson's disease. Neurotox Res. 2020;37:210–26. doi: 10.1007/s12640-019-00097-9.
[89] Kurttio P, Vartiainen T, Savolainen K. Environmental and biological monitoring of exposure to ethylenebisdithiocarbamate fungicides and ethylenethiourea. Occup Env Med. 1990;47:203–6. doi: 10.1136/oem.47.3.203.
[90] Lee K, Park E-K, Stoecklin-Marois M, Koivunen ME, Gee SJ, Hammock BD, et al. Occupational paraquat exposure of agricultural workers in large Costa Rican farms. Int Arch Occup Env Health. 2009;82:455–62. doi: 10.1007/s00420-008-0356-7.
[91] Swaen G, van Amelsvoort L, Boers D, Corsini E, Fustinoni S, Vergieva T, et al. Occupational exposure to ethylenebisdithiocarbamates in agriculture and allergy: results from the EUROPIT field study. Hum Exp Toxicol. 2008;27:715–20. doi: 10.1177/0960327108097433.
[92] Baquet ZC, Williams D, Brody J, Smeyne RJ. A comparison of model-based (2D) and design-based (3D) stereological methods for estimating cell number in the substantia nigra pars compacta (SNpc) of the C57BL/6J mouse. Neuroscience. 2009;161:1082–90. doi: 10.1016/j.neuroscience.2009.04.031.
[93] Ip CW, Cheong D, Volkmann J. Stereological estimation of dopaminergic neuron number in the mouse substantia nigra using the optical fractionator and standard microscopy equipment. J Vis Exp. 2017;127:56103. doi: 10.3791/56103.
[94] Clarke ZA, Andrews TS, Atif J, Pouyabahar D, Innes BT, MacParland SA, et al. Tutorial: guidelines for annotating single-cell transcriptomic maps using automated and manual methods. Nat Protoc. 2021;16:2749–64. doi: 10.1038/s41596-021-00534-0.